Biomaterials 33 (2012) 163–170

Contents lists available at SciVerse ScienceDirect

Biomaterials

journal homepage: www.elsevier.com/locate/biomaterials

The role of iron redox state in the genotoxicity of ultrafine superparamagnetic iron oxide nanoparticles

Neenu Singh [a,*], Gareth J.S. Jenkins [a], Bryant C. Nelson [b], Bryce J. Marquis [b], Thierry G.G. Maffeis [c], Andy P. Brown [d], Paul M. Williams [c], Chris J. Wright [c], Shareen H. Doak [a]

[a] Institute of Life Science, College of Medicine, Swansea University, Singleton Park, Swansea SA2 8PP, Wales, UK
[b] National Institute of Standards and Technology (NIST), Material Measurement Laboratory - Biochemical Science Division, 100 Bureau Drive, Gaithersburg, MD 20899, USA
[c] Multi-disciplinary Nanotechnology Centre, College of Engineering, Swansea University, Singleton Park, Swansea SA2 8PP, Wales, UK
[d] Institute for Materials Research, School of Process, Environmental and Materials Engineering, University of Leeds, Leeds LS2 9JT, UK

ARTICLE INFO

Article history:
Received 8 August 2011
Accepted 21 September 2011
Available online 24 October 2011

Keywords:
Genotoxicity
Iron oxide nanoparticles
Oxidation
Biocompatibility
Metal ion release

ABSTRACT

Ultrafine superparamagnetic iron oxide nanoparticles (USPION) hold great potential for revolutionising biomedical applications such as MRI, localised hyperthermia, and targeted drug delivery. Though evidence is increasing regarding the influence of nanoparticle physico-chemical features on toxicity, data however, is lacking that assesses a range of such characteristics in parallel. We show that iron redox state, a subtle though important physico-chemical feature of USPION, dramatically modifies the cellular uptake of these nanoparticles and influences their induction of DNA damage. Surface chemistry was also found to have an impact and evidence to support a potential mechanism of oxidative DNA damage behind the observed responses has been demonstrated. As human exposure to ferrofluids is predicted to increase through nanomedicine based therapeutics, these findings are important in guiding the fabrication of USPION to ensure they have characteristics that support biocompatibility.

© 2011 Elsevier Ltd. All rights reserved.

1. Introduction

Ultrafine superparamagnetic iron oxide nanoparticles (USPION) are a class of nanoparticles (<100 nm) that hold great potential for revolutionising nanomedicine, with the implementation of functionalised USPION in biomedical applications such as MRI, hyperthermia, detoxification of biological fluids and targeted drug delivery [1–4]. Some key features of these agents, primarily their ease of synthesis, biocompatibility and exploitable magnetic properties, have prompted their rapid growth in fabrication and utilization both in therapeutics and diagnostics [5]. In order to maximize the benefits of using USPION in biomedical applications, a suitable surface coating must be applied to mitigate agglomeration, stabilise the iron oxide core in the *in vivo* aqueous environment and to control biodistribution i.e. evasion from the reticulo-endothelial system (RES) [6]. A vast array of polymers (e.g. chitosan, dextran) and bioactive molecules (e.g. enzymes, DNA/RNA) are used for the surface modification/functionalisation of USPION. The most commonly used coating is dextran, a branched polysaccharide comprised of glucose units [7]. Dextran-coated SPION were approved for clinical use by the US Food and Drug Administration (FDA) owing to their biocompatibility and polar interaction with the iron oxide surface [7].

The wide variety of different formulations relating to size, shape, functional group and surface coating can contribute to the unique and specific physical and chemical features of a particular USPION. These varying characteristics, synergistically or in isolation, govern specific toxicological endpoints ranging from apoptosis and impaired mitochondrial function to generation of reactive oxygen species (ROS) and alteration in gene expression profiles [8–11]. For example, dimercaptosuccinic acid (DMSA) stabilised SPION induced toxic effects in PC12 neural cells, while neither DMSA nor the SPION core alone displayed any significant toxicity [12].

Although the importance of nanomaterial physico-chemical characteristics on toxic potential has been well-recognized, the tendency of iron in USPION to undergo oxidation presents an additional complication. Aqueous suspensions of USPION exist mainly as magnetite (Fe_3O_4) or maghemite (γ-Fe_2O_3) [13,14]. Magnetite (also written as, $FeO.Fe_2O_3$) contains both Fe^{2+} and Fe^{3+} ions and is thermodynamically unstable because the Fe^{2+} in the crystalline lattice can readily undergo oxidation, forming a product in the solid solution range between magnetite and maghemite in the presence of air, light and moisture [15]. Therefore, as a common by-product of magnetite oxidation,

* Corresponding author. Tel.: +44 1792 295388; fax: +44 1792 602147.
E-mail address: n.singh@swansea.ac.uk (N. Singh).

0142-9612/$ – see front matter © 2011 Elsevier Ltd. All rights reserved.
doi:10.1016/j.biomaterials.2011.09.087

maghemite or a non-stoichiometric intermediate can potentially be found in ferrofluids.

The two forms of iron oxides can demonstrate different cellular responses. In fact, uncoated Fe_3O_4 nanoparticles can cause higher levels of oxidative DNA lesions in lung epithelial cells than uncoated γ-Fe_2O_3 nanoparticles [16,17]. On the other hand, γ-Fe_2O_3 can cause cell death and ROS production in endothelial cells [18], while Fe_3O_4 nanoparticles have been associated with biocompatibility and lack of toxicity [19,20]. However, these materials were investigated in different studies and thus, slight differences in their physico-chemical features may also contribute to the different cellular responses observed.

In the present study, we employed four different USPION with the same core particle size to examine whether other physico-chemical characteristics including surface coating and most importantly, the iron redox state could modulate cellular internalisation and genotoxicity.

2. Materials and methods

2.1. Materials

Dextran-coated USPION (dUSPION), including Fe_3O_4 dUSPION, γ-Fe_2O_3 dUSPION and powders of uncoated Fe_3O_4 and uncoated γ-Fe_2O_3 were purchased from Liquids Research, Bangor, UK. RPMI 1640, horse serum and L-glutamine, sodium pyruvate, antibiotics were purchased from Gibco, UK. N-acetyl-L-cysteine (NAC), dimethyl sulphoxide (DMSO), L-ascorbic acid sodium salt, ferrozine (3-(2-pyridyl)-5,6-bis(phenyl sulfonic acid)-1,2,4-triazine), pyridine and neocuproine (2,9-dimethyl(1,10-phenanthroline) were obtained from Sigma-Aldrich, UK.

Human lymphoblastoid cell line (MCL-5) was purchased from Genetest Corporation and cultured in RPMI-1640 supplemented with 10% horse serum and 1% L-glutamine. Human foreskin fibroblast cell line (HFF-1) was purchased from American Type Culture Collection (Manassas, VA, USA) and cultured in DMEM (with 4.5 g/L glucose) supplemented with 15% foetal calf serum, 1% sodium pyruvate (1 mM) and 1% streptomycin (100 $\mu g\ ml^{-1}$)/penicillin (100 IU ml^{-1}).

The stable isotope-labeled modified DNA base standards, thymine glycol-d_4 [TG-d_4], 5-hydroxy-5-methylhydantoin-$^{13}C\ ^{15}N_2$ [5-OH-5-MeHyd-$^{13}C\ ^{15}N_2$], 2,4-diamino-5-formamidopyrimidine-$^{13}C\ \ ^{15}N_2$ [FapyAde-$^{13}C\ ^{15}N_2$], 2,6-diamino-4-hydroxy-5-formamidopyrimidine-$^{13}C\ ^{15}N_2$ [FapyGua-$^{13}C\ ^{15}N_2$] and 8-hydroxyguanine-$^{15}N_5$ [8-OH-Gua-$^{15}N_5$] were obtained from Cambridge Isotope Laboratories, Inc. (Andover, MA). Formamidopyrimidine-DNA gylcosylase (Fpg) and endonuclease III (EndoIII) were expressed and purified from E. coli as previously described [21,22]. Bis(-trimethylsilyl)trifluoroacetamide(BSFTA)/1% trimethylchlorosilane was purchased from Pierce Chemical Co. (Rockford, IL).

2.2. Dynamic light Scattering (DLS)

The hydrodynamic particle sizes of USPION samples were obtained by DLS. The measurements were performed using a Malvern 4700 spectrometer (Malvern instruments Ltd., UK) in water, horse serum and RPMI-1640 medium with 1% or 10% horse serum. Data are presented as the average of 10 readings.

2.3. X-ray Photoelectron Spectroscopy (XPS)

The oxidation state of iron in all four USPION was confirmed by XPS [23]. XPS of the uncoated powders was carried out in a VG Escalab using Al Kalpha unmonochromated radiation (1486.3 eV). The powders were pressed into Indium foil and scanned. The Fe^{2+}/Fe^{3+} ratio was extracted from the Fe2p and Fe3p core level, scanned at a pass energy of 10 eV.

2.4. Zeta potential

The ζ-potential values of the USPION were determined by Zetasizer 2000 (Malvern instruments Ltd., UK). The nanoparticles were dispersed in water or 1% serum medium and the ζ-potential values presented are the average of 10 readings.

2.5. Transmission Electron Microscopy (TEM)

USPION samples for TEM were prepared, as previously described [24]. *Sample preparation*: Subsequent to treatment with either of the four dUSPION the cells were washed twice in serum free medium, re-suspended in 3% glutaraldehyde buffer solution (1.2 ml of 25% glutaldehyde in 10 ml of 0.1 M cacodylate buffer) for 2 h at 4 °C. The cells were then centrifuged, and the pellet was re-suspended in 0.1% glutaraldehyde and stored at 4 °C. Cell preparations were processed for TEM analysis following the method as described previously [24]. TEM analysis was undertaken with a FEI/Philips CM200 field emission gun TEM operating at 197 keV and fitted with a Gatan Imaging Filter (GIF 200) and an Oxford Instruments ultrathin window energy dispersive X-ray detector (EDX).

2.6. Micronucleus assay

The sequential cytokinesis-blocked micronucleus (CBMN) assay was performed as recommended by Doak et al. (2009) [25]. Briefly, $1x10^5$ cells per ml were seeded for 24 h. The cells were then exposed to the USPION samples for 24 h in 1% serum containing medium. The concentration of USPION used in this study is relevant to the dosages employed in clinical trials [9,26]. Mitomycin-C (MMC) 0.01 $\mu g\ ml^{-1}$ was used as an assay positive control and all treatments were performed in duplicates. Following exposure, cell preparations were washed and incubated for further 24 h with 10% serum medium containing 3 $\mu g\ ml^{-1}$ cytochalasin B. The cells were harvested (see Supplementary Methods) and stained with 4′,6-diamidino-2-phenylindole (DAPI).

Relative population doubling (RPD) was used to assess cytotoxicity (see Supplementary Methods) [27]. High numbers of cells (5000 per dose) were scored in the CBMN assay in an automated manner using the Metafer image analysis system (MetaSystems, Carl Zeiss Ltd) to enhance assay sensitivity and statistical power (routine analysis requires scoring 2000 cells per dose; OECD 487).

To assess the role played by oxidative stress in inducing DNA damage, cells were pre-treated with 2 mM of the anti-oxidant, N-acetyl-L- Cysteine (NAC) for 2-h, followed by γ-Fe_2O_3 dUSPION for 24-h before performing the CBMN assay as described above.

2.7. Kinetochore staining

Following CBMN assay treatment, the cells were cytocentrifuged onto slides and fixed in 90% methanol at −20 °C. Immunofluorescent staining of kinetochore proteins was performed as described by Ellard et al. [28] except that counterstaining was with DAPI (Vectashield; Vector Laboratories, UK). Kinetochore scoring was carried out on a Zeiss AxioCam HRc (Carl Zeiss Microscopy and Imaging, UK). For each dose, micronuclei from 100 binucleated cells were scored for the presence or absence of kinetochore signals.

2.8. DNA damage measurements using Gas chromatography/mass spectrometry (GC/MS)

GC/MS with isotope dilution was used to determine the absolute levels of five different oxidized base products: 8-OH-Gua, TG, 5-OH-5-MeHyd, FapyGua and FapyAde. MCL5 cells were seeded for 24 h at $1x10^5$ cells per ml, then treated with γ-Fe_2O_3 dUSPION for a further 24 h. Following washing, DNA was extracted from the treated cells using the DNeasy Blood & Tissue Kit (Qiagen). The DNA was precipitated and GC/MS analysis was performed as described by previously [29](see Supplementary Methods).

2.9. Ferrozine assay

The ferrozine assay was performed as described by Riemer et al. [30]. Briefly, the cell pellets were lysed in 200 μL of 0.01 M HCl and 100 μL of the iron-releasing reagent (a freshly mixed solution of equal volumes of 2.4 M HCl and 9% (w/v) $KMnO_4$ in H_2O), for 2 h at 60 °C. After cooling to room temperature, 20 μL of the iron-detection reagent [162.5ul ferrozine (6.5 mM), 164ul neocuproine (13.1 mM), 1.66 ml ammonium acetate (5 M), and 0.88 g ascorbic acid and 500 μL of water] was added to each tube and vortexed before transferring into a 96-well plate for absorbance measurement at 550 nm. Iron content was determined by calibration against a standard curve made using ferrous ethylenediammonium sulphate (Ferrous EAS). All experiments were performed in triplicate.

2.10. Determination of free ferric ion (Fe^{3+})

In order to measure free Fe^{3+} ions, citrate buffer with different pH (4.5, 5.5 and 7) was made as described by Arbab et al. [31] γ-Fe_2O_3 dUSPION was diluted to a concentration of 100 $\mu g\ ml^{-1}$ in the different buffer systems) in a total volume of 1 ml and the mixtures were incubated at 37 °C (5% CO_2) for 24, 48 72 and 96 h. At each time point, 200 μl was taken and diluted to 4 ml in PBS. 0.4 ml of this mixture was added to 25 μM Tiron, 500 μl KOH(4 N) and 1 ml of phosphate-containing buffer (as described by Soenen et al. [32]). The absorbance was then measured at 490 nm. The concentration of Fe^{3+} ions in solution after incubation of USPION in buffers of different pH was calculated by subtracting the concentration obtained from γ-Fe_2O_3 dUSPION without any pH buffer.

2.11. Statistical analysis

In the MN assay duplicates of each dose were used and statistical significance was determined according to the Fisher's exact test. Statistically significant accumulation of DNA base oxidative lesions was assessed via one-way ANOVA with posthoc Dunnett's multiple comparison test (GraphPad Prism 5.0, La Jolla, CA). In the

ferrozine assay, student's *t*-test was used to compare the differences between the means of two samples. Differences were deemed to be significant when $p < 0.05$.

3. Results

3.1. Physico-chemical characterisation

A range of physico-chemical properties were characterised for all the USPION under study (Table 1). TEM was used to determine size, morphology and crystallinity of the USPION. All were ~10 nm in size, had a crystalline core with an inverse spinel structure and had similar near-spherical morphology except for the additional presence of some nanorods in the uncoated γ-Fe_2O_3. The DLS measurements revealed that in the presence of 10% serum containing media (vs. 1% serum containing media or water), the hydrodynamic size of all the USPION was at the lowest (~100 nm), the difference being most pronounced for the uncoated USPION samples. Agglomeration of the uncoated USPION samples was considerably higher in water than serum containing media. The zeta potential for all USPION were between −13.9 ± 1.4 mV and 3.3 ± 0.4 mV and therefore, considered approximately neutral [33]. EDX indicated the presence of only iron and oxygen in the uncoated USPION and iron, oxygen and carbon in the case of dUSPION. Note that due to the ease of Fe_3O_4 oxidation, these samples were rarely pure when supplied by the manufacturer and indeed were mixed Fe_3O_4/γ-Fe_2O_3 samples.

3.2. Effect of serum concentration on cellular uptake of USPION

MCL5 cells were treated with 100 μg ml^{-1} of γ-Fe_2O_3 dUSPION, Fe_3O_4 dUSPION, uncoated Fe_2O_3 or uncoated Fe_3O_4 in 1% or 10% serum containing medium for 24 h. Intracellular iron content was determined by the ferrozine assay and confirmed by TEM. Treatment with γ-Fe_2O_3 dUSPION in 1% (*vs.* 10%) serum medium brought about a substantial increase in cellular uptake (Fig. 1a) and this was confirmed by TEM analysis, which showed these USPION largely localised within vesicles although some non-membrane bound nanoparticles were observed in the cytoplasm (Fig. 1b). Similar observations under varying serum conditions were made on the HFF-1 fibroblast cell line after exposure to Fe_2O_3 dUSPION i.e. significant increase in cellular iron content in 2% *vs.* 15% serum medium (results not shown). The other USPION samples examined did not show significant uptake in 1% *vs.* 10% serum supplemented media (Fig. 1a). In fact, in the presence of 10% serum medium, MCL5 cells exhibited similar cellular iron content levels regardless of the USPION sample exposure.

3.3. Genotoxicity in MCL5 cells exposed to USPION

MCL5 cells were treated with a range of concentrations (1–100 μg ml^{-1}) of γ-Fe_2O_3 dUSPION, Fe_3O_4 dUSPION, uncoated γ-Fe_2O_3 or uncoated Fe_3O_4 in 1% serum medium for 24 h in order to assess USPION induced chromosomal damage (Fig. 2). No cytotoxicity was observed over the selected dose-range with any of the USPION samples studied and the only sample to demonstrate genotoxicity was γ-Fe_2O_3 dUSPION (Fig. 2a).

A no-observed effect level (NOEL) was observed for γ-Fe_2O_3 dUSPION exposures between 0 and 3 μg ml^{-1} and above this statistically significant increases in chromosomal damage were observed, resulting in a lowest-observed effect level (LOEL) at 4 μg ml^{-1} ($P < 0.01$). At 4 μg ml^{-1}, the micronuclei frequency was elevated to 2.5 *vs.* 1.1 for control; subsequent higher doses of γ-Fe_2O_3 dUSPION above the LOEL, did not result in further substantial increases in chromosomal damage (Fig. 2a). Whilst γ-Fe_2O_3-dUSPION induced significant micronuclei at a concentration of 4 μg ml^{-1} and higher, Fe_3O_4-dUSPION, uncoated Fe_3O_4 and uncoated γ-Fe_2O_3 did not induce micronuclei above control at any of the concentrations tested (Fig. 2b–d). In addition, no increase in frequency of micronuclei or cytotoxicity was observed upon exposure of MCL5 cells with dextran only (results not shown).

Kinetochore staining following the CBMN assay was performed to identify micronuclei containing a centromere (kinetochore positive; K+) indicating the presence of a whole chromosome; or lacking a centromere (kinetochore negative, K-), which represents chromosome fragments within the micronucleus. The ratio of K- to K+ micronuclei was therefore, determined. Fig. 2e, shows the

Table 1
Summary of physico-chemical characterisation data for maghemite dUSPION, magnetite-dUSPION, uncoated maghemite and uncoated magnetite. $N = 10$. [maghemite = γ-Fe_2O_3; magnetite = Fe_3O_4]. All had an inverse spinel structure (by electron diffraction) and had similar near-spherical morphology except for the additional presence of some nanorods in the uncoated γ-Fe_2O_3.

Physico-chemical characteristics	γ-Fe_2O_3 dUSPION	Fe_3O_4 dUSPION	Uncoated γ-Fe_2O_3	Uncoated Fe_3O_4
Particle morphology	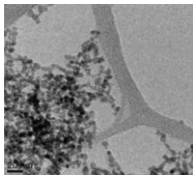	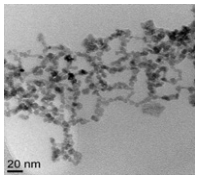	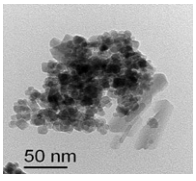	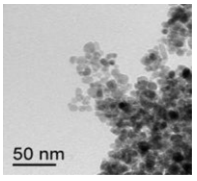
Primary particle size	10 nm Crystalline	10 nm Crystalline	10–20 nm Crystalline	10 nm Crystalline
Hydrodynamic diameter (nm)				
• Water	75 ± 2.5 nm	160 ± 8 nm	3900 ± 300 nm	1450 ± 132 nm
• 1% serum medium	80 ± 5 nm	156 ± 1 nm	819 ± 87 nm	905 ± 204 nm
• 10% serum medium	57.5 ± 11 nm	112 ± 2 nm	101 ± 19.6 nm	107 ± 23 nm
Zeta potential				
• Water	−11.4 ± 2.5 mV	−11.4 ± 1.6 mV	−13.9 ± 1.4 mV	3.3 ± 0.4 mV
• 1% serum medium	−4.1 ± 1.0 mV	4.7 ± 1.3 mV	−8.7 ± 3.4 mV	−9.2 ± 2.2 mV
• 10% serum medium	−4.8 ± 1.2 mV	4.2 ± 1.1 mV	−7.9 ± 1.7 mV	−7.9 ± 1.5 mV
Chemical Composition	$Fe^{2+}/Fe^{3+} = 0.118$	$Fe^{2+}/Fe^{3+} = 0.435$	Only Fe^{3+} detected	$Fe^{2+}/Fe^{3+} = 1.22$

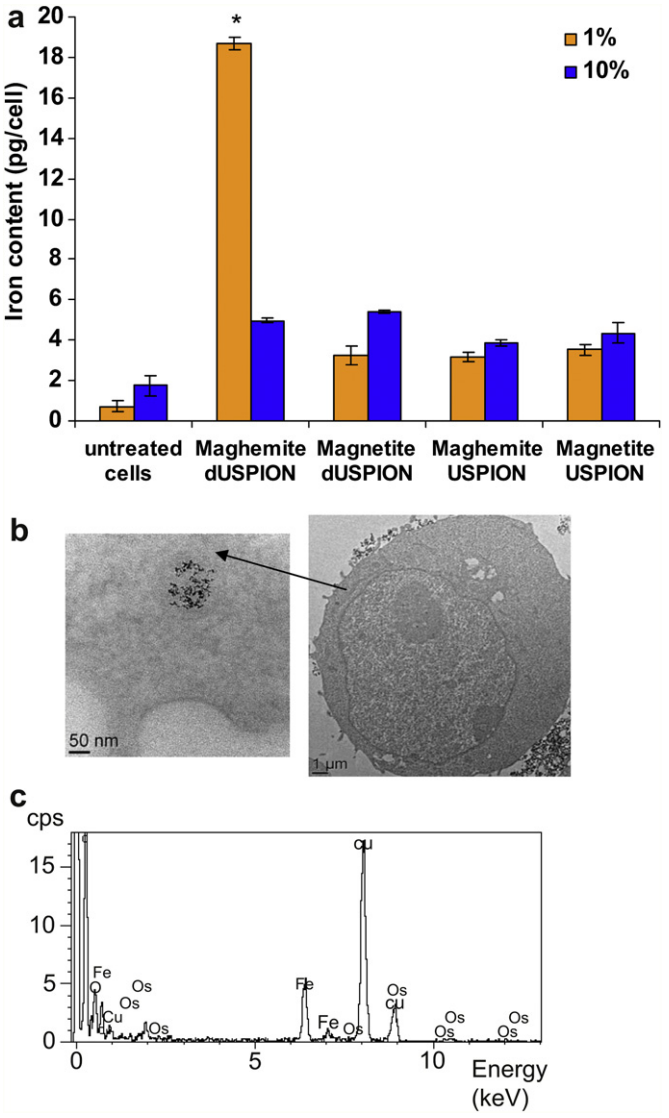

Fig. 1. Effect of serum concentration on cellular uptake of different USPION. (a) Iron content (pg/cell) in MCL5 cells following 24 h exposure (100 μg ml^{-1}) to γ-Fe_2O_3 dUSPION, Fe_3O_4 dUSPION, uncoated γ-Fe_2O_3 or uncoated Fe_3O_4 in the presence of 1% or 10% serum, measured using the ferrozine assay. Data are expressed as mean ± standard deviation. b) Representative TEM image of MCL5 cell treated with γ-Fe_2O_3 dUSPION. The magnified box shows USPION located within the vesicles (c) Energy-dispersive X-ray analysis of γ-Fe_2O_3 showing Fe and O peaks (the copper and osmium peaks are background signals from the support film and specimen holder). $^*p < 0.01$ when compared to cellular uptake in 10% serum medium or other USPION at both serum concentrations. $N = 3$.

percentage of both K+ and K- that contribute to the total percentage of micronuclei at a given dose of γ-Fe_2O_3 dUSPION. As expected, the frequency of K+ and K- centromeres was similar in the untreated cells as any micronuclei are generated through a random damaging event. In the γ-Fe_2O_3 dUSPION treated cells however, the proportion of K- micronuclei increased at 4 μg ml^{-1} and this increase was sustained at all the higher concentrations studied indicating the predominant induction of chromosome fragmentation by exposure to γ-Fe_2O_3 dUSPION.

3.4. Role of oxidative stress in inducing DNA damage

MCL5 cells were treated with 0, 2 or 4 μg ml^{-1} of γ-Fe_2O_3 dUSPION in 1% serum medium for 24 h and the extracted DNA was analyzed with GC/MS in order to quantify the levels of accumulated oxidative base lesions. As shown in Fig. 3a, dose-dependent increases in the levels of 8-OH-Gua, FapyGua and TG were observed. The level of FapyAde was also increased but only at the highest dose. Furthermore, four of the five detected lesions were significantly increased at the highest γ-Fe_2O_3 dUSPION dose.

The GC/MS study clearly demonstrated that exposure to γ-Fe_2O_3 dUSPION resulted in oxidative damage to DNA. To determine if these oxidative lesions were directly responsible for the genotoxicity observed with the CBMN assay (Fig. 2a), the 4 μg ml^{-1} and 50 μg ml^{-1} doses were chosen to study the effect of the reactive oxygen species (ROS) scavenger, N-acetyl-L-cysteine (NAC). MCL5 cells were pre-treated with or without NAC (2 mM) for 2 h prior to repeating the CBMN assay. As shown in Fig. 3b, pre-treatment with NAC, significantly reduced the micronuclei frequency in MCL5 cells when compared to cells with no ROS scavenger pre-treatment. The data suggest that dUSPION induced ROS have a direct role in the induction of chromosomal damage and the subsequent formation of micronuclei.

3.5. Effect of pH on the generation of Fe^{3+} ions in γ-Fe_2O_3 dUSPION

As the TEM imaging revealed that the of γ-Fe_2O_3 dUSPION were largely enclosed within membrane bound vesicles, we wished to examine the possibility that the NP may release Fe^{3+} ions (particularly within low pH lysosomes). Thus, 100 μg ml^{-1}of γ-Fe_2O_3 dUSPION were incubated for 24, 48, 72 and 96 h in citrate buffers at different pH (i.e. 4.5, 5.5 and 7). As shown in Fig. 4, there was a pH and time-dependent release of Fe^{3+} ions resulting in a substantial significant increase at longer times and lower pH (20.3 μg ml^{-1} at 72 h followed by 28.5 μg ml^{-1} at 96 h, at pH 4.5). At all time points, there was a significant increase in ferric ions at pH 4.5 as compared to that at higher pH.

4. Discussion

This study is the first to provide evidence that the redox state of iron in USPION, in conjunction with other well–known physicochemical properties such as agglomerate size and surface coatings can dramatically modify the cellular uptake and inherent (geno)toxicity profile of SPION. Despite the notable attributes of SPION including biocompatibility and the body's intrinsic iron homeostatic mechanisms for efficient clearance from the body, the physico-chemical properties of SPION play a key role in influencing their pharmacokinetic behaviour. This ultimately determines their *in vivo* fate and therefore, necessitates their thorough physicochemical characterisation and safety assessment [34,35].

Cyto- and/or genotoxicity can be indirectly influenced by the interaction between nanoparticles (NP) and the culture growth medium, which comprises an array of proteins, nutrients and growth factors [25]. Both *in vitro* and *in vivo*, the nanoparticle–protein corona is likely to be a complex entity that is transient in nature and is largely determined by the extracellular environment (culture media or body fluids), as well as the physicochemical properties of the NP itself [36]. These protein associations could potentially govern cellular interactions including NP-cell adhesion, intracellular uptake and localization, besides modulating downstream cellular responses, such as oxidative stress and genotoxicity.

Indeed, in the present study, the significantly greater cellular uptake of γ-Fe_2O_3 dUSPION was shown to be associated with the serum concentration of the medium, with the low serum concentration having a positive influence on uptake (Fig. 1). This observation was nanoparticle specific and did not hold true for the other UPSION studied, where little difference in uptake was observed

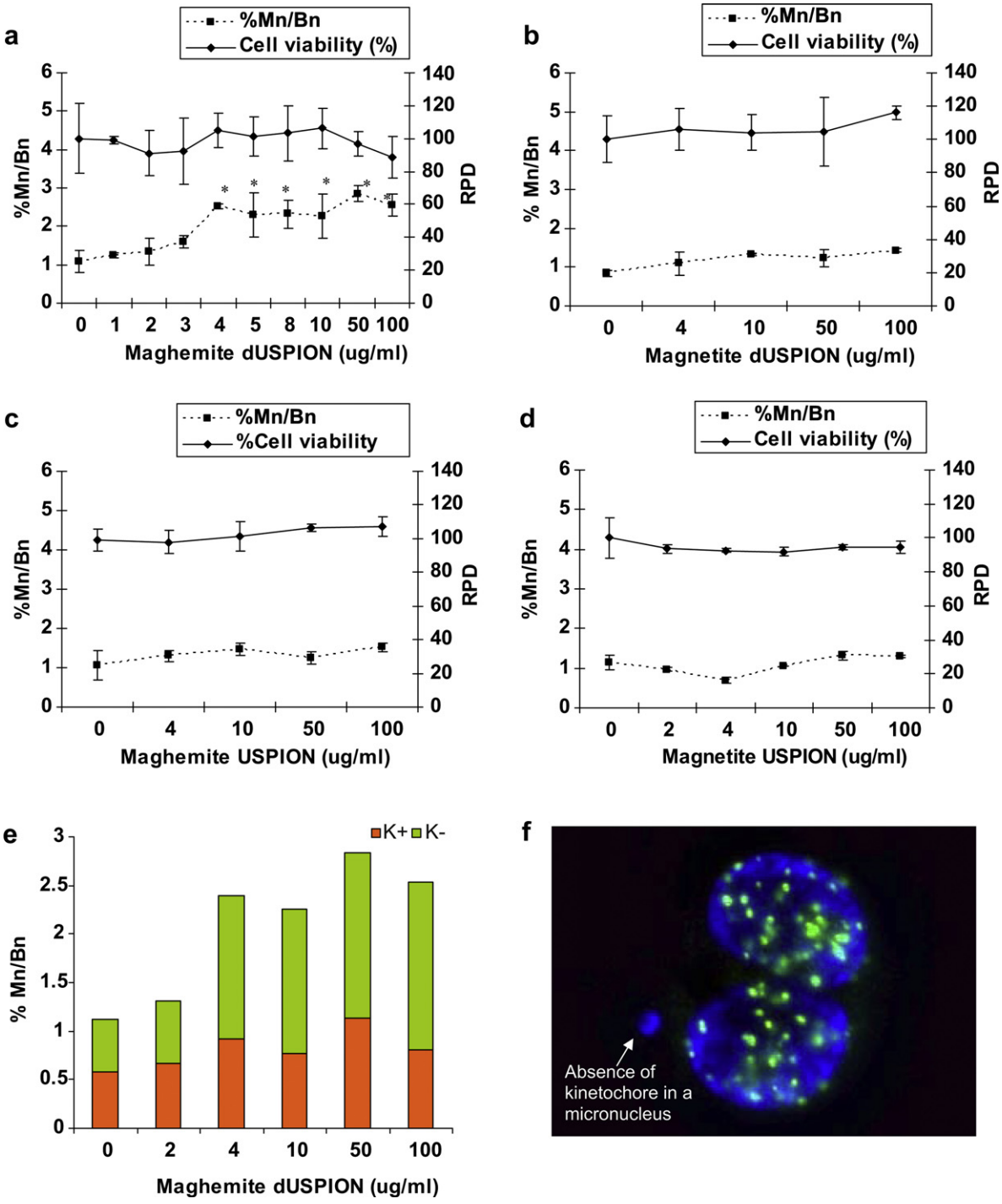

Fig. 2. Micronucleus frequency and cell viability in MCL5 cells exposed to different USPION doses. (a) γ-Fe_2O_3 dUSPION (b) Fe_3O_4 dUSPION (c) uncoated γ-Fe_2O_3 (d) uncoated Fe_3O_4. Micronucleus frequency was measured by calculating the percentage of micronuclei in binucleated cells (%Mn/Bn) per exposure dose. Cell viability was measured based on relative population doubling (RPD) (*$p < 0.05$ as compared to the frequency of micronuclei in the control). (e) Kinetochore staining: Frequency of kinetochore negative (K-) micronuclei and kinetochore positive (K+) micronuclei in MCL5 cells treated with γ-Fe_2O_3 dUSPION at 0, 2, 4, 10, 50 and 100 μg ml^{-1}, $N = 100$ micronuclei in binucleated cells. (f) Kinetochore staining showing clastogenicity (chromosome fragmentation).

regardless of serum concentration in the media. It is tempting to suggest in the light of the data presented here that the oxidation state of iron and the dextran surface coating may synergistically modulate the cellular internalisation of the different USPION used in the present study and it is the combination that play a key role in the observed differential cellular uptake [37]. The cellular uptake of γ-Fe_2O_3 dUSPION may be a consequence of the plausible interaction of the serum components with the dextran-coated γ-Fe_2O_3 and/or the adsorption of serum proteins onto these nanoparticles; this could alter the hydrodynamic diameter or the cell surface- γ-Fe_2O_3 dUSPION electrostatic interactions and thus, largely influence the uptake of these particles [25]. Lack of internalisation of the other USPION may be due to factors such as potential agglomeration (DLS measurements show γ-Fe_2O3

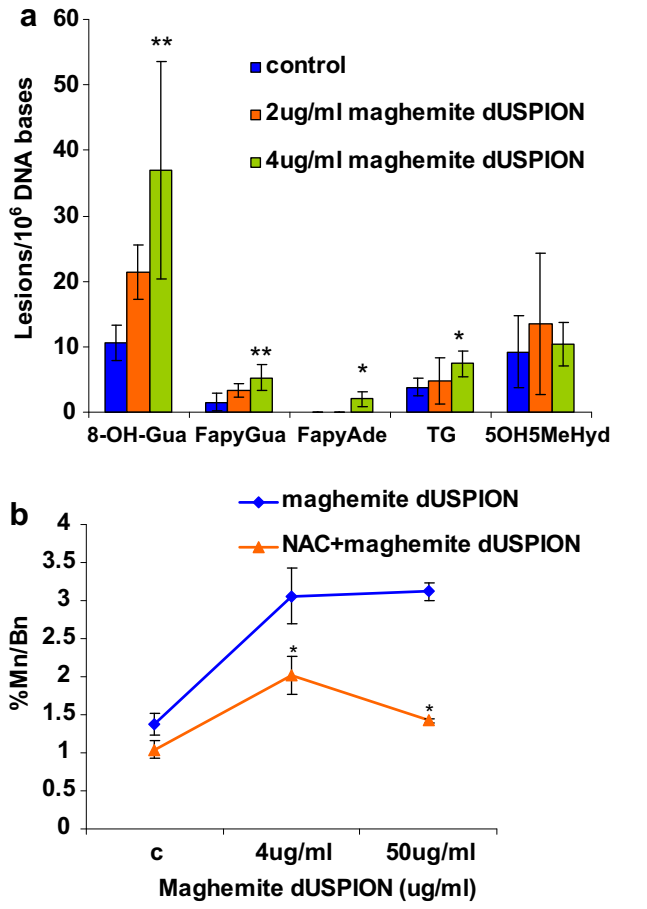

Fig. 3. Role of oxidative stress in causing DNA damage in MCL5 cells: (a) DNA lesions: 8-OH-Gua, FapyGua, FapyAde,TG and 5-OH-5MeHyd were assessed using GC/MS. $^{*}p < 0.05$ and $^{**}p < 0.01$ compared to untreated cells. All data points represent the mean of 5 independent measurements. Uncertainties are standard deviations. (b) Effect of NAC on micronuclei frequency in MCL5 cells. Micronucleus frequency was measured by calculating the percentage of micronuclei in binucleated cells (%Mn/Bn). $^{*}p < 0.05$, when comparing γ-Fe_2O_3 dUSPION treatment plus NAC to their corresponding γ-Fe_2O_3 dUSPION treated cells.

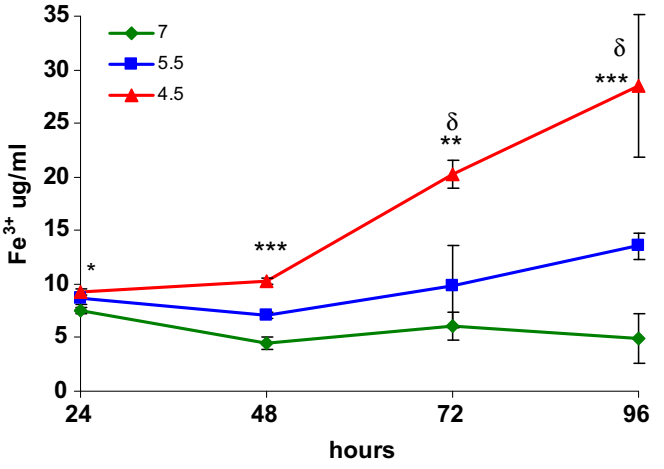

Fig. 4. Effect of pH on the generation of Fe^{3+} ions in γ-Fe_2O_3 dUSPION: The amount of Fe^{3+} ions was measured over a period of 96 h at different pH values i.e. 7, 5.5 and 4.5. The pH dependent release is maximal and significantly increased at pH 4.5 as compared to pH = 7 [$^{*}p < 0.05$; $^{**}p < 0.01$, $^{*}p < 0.001$]. The release of Fe^{3+} ions is also time-dependent (72–96 h *vs.* 24–48 h)[$^{\delta}$ $p < 0.01$]. The values for free Fe^{3+} ions are obtained by subtracting value of Fe^{3+} ions obtained in the absence of any buffer. $N = 3$.

dUSPION to have the smallest hydrodynamic agglomerate size; Table 1) and adsorption of proteins that negatively regulate cellular uptake.

Several studies have reported the influence of serum on cellular uptake. For example, the presence of serum is responsible for decreased cellular uptake of γ-Fe_2O_3 nanoparticles and silica-coated particles in the HeLa cell line but an opposite effect was observed in macrophages [38,39]. In support of the protein-NP interaction, pre-incubation of uncoated-SPION with the culture media prior to the assessment of cytotoxicity results in decreased toxicity [40]. It is believed that a masked reactive surface of the uncoated USPION could minimise the adverse cell–NP and/or serum protein–NP interactions resulting in decreased cytotoxicity and possibly reduced cellular uptake as observed in the present study.

Of significant interest, the present study showed that cellular internalisation of γ-Fe_2O_3 dUSPION positively correlated with the induction of genotoxicity (Fig. 2). The results indicate that exposure of γ-Fe_2O_3 dUSPION to MCL5 cells showed a significant increase in micronuclei frequency from a dose of 4 μg ml^{-1}, with no cytotoxicity observed up to the maximum dose of 100 μg ml^{-1}. Similarly, SPION coated with meso-2,3-dimercaptosuccinic acid (DMSA) induced genotoxicity (using the comet assay) at concentrations of 10–100 μg ml^{-1} in the absence of significant cytotoxicity [10]. Further investigation using kinetochore labelling, subsequently demonstrated that the ratio of kinetochore negative to positive micronuclei was higher than the untreated cells at all exposure doses above 4 μg ml^{-1} of γ-Fe_2O_3 dUSPION, demonstrating that chromosomal damage was primarily via DNA fragmentation, indicating a clastogenic mode of micronuclei formation (Fig. 2e).

One of the key and perhaps the most broadly developed mechanisms thought to be responsible for cellular damage induced by USPION is the generation of oxidative stress, which is usually the consequence of the production of ROS, such as the highly reactive hydroxyl radical ($^{\bullet}$OH). $^{\bullet}$OH attack on DNA can lead to single and double strand breaks and to the accumulation of a variety of mutagenic and/or cytotoxic lesions [41]. Indeed, in the current study, exposure to 4 μg ml^{-1} of γ-Fe_2O_3 dUSPION resulted in the formation and accumulation of a series of oxidative DNA lesions, which corresponded to the dose required for the first significant increase in micronuclei (Fig. 3a). Though the lower dose of 2 μg ml^{-1} did cause an increase in lesions, the levels were not statistically significant and as no increase in micronuclei frequency was detected at this dose, the data suggest that the cells were able to effectively tolerate or repair the DNA damage.

The present study, not only found oxidative DNA lesions but also demonstrated that the addition of NAC, was able to significantly reduce the frequency of micronuclei γ-Fe_2O_3 dUSPION exposed cells (Fig. 3b). This clear association provides evidence for the role of free radical-based damage in inducing genotoxicity. Pre-treatment of human endothelial cells with NAC, can inhibit the induction of ROS by quantum dots and subsequent DNA double strand breaks as measured by the formation of phosphorylated histone protein gamma H2AX nuclear foci [42]. Titanium dioxide nanoparticles can induce ROS-mediated genotoxicity as measured by the Fpg-modified Comet assay and micronucleus formation in human epidermal cells [43]. For a recent overview of studies focused on nanoparticle induced oxidative stress and the resulting mechanisms of genotoxicity, readers are referred to the review by Petersen and Nelson [41].

This study indicates attack by $^{\bullet}$OH following exposure to SPION and an obvious source of $^{\bullet}$OH is via Fenton chemistry from iron ions [44]. Cellular exposure to/uptake of SPION could result in its degradation/dissolution to release Fe ions fuelling the generation of ROS and resultant genotoxicity. These ions in their free unbound

form, can catalyze Haber–Weiss and/or Fenton reactions to generate ROS which, can eventually lead to oxidative damage to biomolecules, affect cell functionality, reduced MR contrast and may cause DNA damage as seen in the present study [32].

In order to explore the potential for dissolution of USPION in the cellular environment, this study investigated the generation of Fe^{3+} ions over time using a lysosomal model system [31] With the model we have demonstrated a pH and time-dependent release of Fe^{3+} ions by γ-Fe_2O_3 dUSPION (Fig. 4). If USPION entering the cell do so by endocytosis (as observed here), the particles are exposed to a range of different pH from 7.4 in the extracellular milieu to 5.5 in the early endosomes and 4.5 in the late endosomes. Thus, it is highly unlikely the particles broke down in the media but could very well have released metal ions when inside the cells, enclosed in vesicles. These Fe^{3+} ions can potentially escape into the cytoplasm and form part of accessible iron ions called the labile iron pool (LIP), which has also been shown to exist in the nucleus [45,46]. LIP is not only a source of iron ions available for Fenton reaction, but its levels are associated with the production of 8-OH-Gua in the lymphocytes [47].

The generation of Fe ions, chromosomal damage due to DNA fragmentation and accumulation of oxidized DNA bases lesions, all suggest a mechanism of oxidative DNA damage by γ-Fe_2O_3 dUSPION. During the synthesis of USPION and subsequent environmental oxidation/reduction reactions, the composition with respect to the oxidation state of iron can vary considerably across the solid solution range of Fe_3O_4 to γ-Fe_2O_3 [48]. Thus the varying redox potential and surface coordination chemistries that ensue from the non-stoichiometric ratios of Fe^{2+} and Fe^{3+} may eventually promote the observed differential uptake, oxidative stress and the corresponding genotoxicity [15].

5. Conclusions

In summary, this study demonstrates that the redox state of iron in USPION is a critical feature to be taken into consideration when assessing cellular damage end-points. The serum/medium components play an important role in cellular uptake of the γ-Fe_2O_3 dUSPION and showed a correlation to the induction of DNA damage. γ-Fe_2O_3 dUSPION-induced genotoxicity, was a direct consequence of oxidative stress related damage that could potentially lead to the initiation and progression of cancer. Since human exposure to ferrofluids is predicted to increase in nanomedicine based therapeutics, these findings warrant the need to devise rigorous testing strategies, in terms of thorough physico-chemical characterisation. This will ensure whether a given ferrofluid has incorporated any changes in its oxidation state and composition, which could influence its cellular interaction and the ensuing downstream genotoxicity. Alternatively, it may be necessary to design iron oxide nanoparticles that are highly stable chemically and oxidation resistant to avoid compromising cellular integrity.

Acknowledgements

This work is supported by funds from the Medical Research Council and the Research Councils UK (SHD Academic Fellowship).The authors wish to acknowledge EPSRC (EP/E059678/1 and EP/H008578/1) for financial support. TEM results were obtained using the Leeds EPSRC Nanoscience and Nanotechnology Research Equipment Facility (EP/F056311/1). The authors also wish to thank Dr Alice Warley, Dr Anthony Brain and Mr Ken Brady (Centre for Ultrastructural Imaging, King's College London) for expert sample preparation. We are also grateful to Prof. Andrew Barron and Mr Alvin Orbaek (Chemistry Department, Rice University) for XPS data analysis and interpretation.

NIST Disclaimer: Certain commercial equipment, instruments and materials are identified in this paper to specify an experimental procedure as completely as possible. In no case does the identification of particular equipment or materials imply a recommendation or endorsement by the National Institute of Standards and Technology nor does it imply that the materials, instruments, or equipment are necessarily the best available for the purpose.

Appendix. supplementary material

Supplementary material related to this article can be found online at doi:10.1016/j.biomaterials.2011.09.087.

References

[1] Bulte JW, Douglas T, Witwer B, Zhang SC, Strable E, Lewis BK, et al. Magnetodendrimers allow endosomal magnetic labeling and in vivo tracking of stem cells. Nat Biotechnol 2001;19(12):1141–7.
[2] Bulte JW, Kraitchman DL. Iron oxide MR contrast agents for molecular and cellular imaging. NMR Biomed 2004;17(7):484–99.
[3] Gupta AK, Gupta M. Synthesis and surface engineering of iron oxide nanoparticles for biomedical applications. Biomaterials 2005;26(18):3995–4021.
[4] Pamme N, Wilhelm C. Continuous sorting of magnetic cells via on-chip free-flow magnetophoresis. Lab Chip 2006;6(8):974–80.
[5] Weinstein JS, Varallyay CG, Dosa E, Gahramanov S, Hamilton B, Rooney WD, et al. Superparamagnetic iron oxide nanoparticles: diagnostic magnetic resonance imaging and potential therapeutic applications in neurooncology and central nervous system inflammatory pathologies, a review. J Cereb Blood Flow Metab 2010;30(1):15–35.
[6] Soenen SJ, De Cuyper M. Assessing iron oxide nanoparticle toxicity in vitro: current status and future prospects. Nanomedicine (Lond) 2010;5(8):1261–75.
[7] Veiseh O, Gunn JW, Zhang M. Design and fabrication of magnetic nanoparticles for targeted drug delivery and imaging. Adv Drug Deliv Rev 2010;62(3):284–304.
[8] Song MM, Song WJ, Bi H, Wang J, Wu WL, Sun J, et al. Cytotoxicity and cellular uptake of iron nanowires. Biomaterials 2010;31(7):1509–17.
[9] Apopa PL, Qian Y, Shao R, Guo NL, Schwegler-Berry D, Pacurari M, et al. Iron oxide nanoparticles induce human microvascular endothelial cell permeability through reactive oxygen species production and microtubule remodeling. Part Fibre Toxicol 2009;6:1.
[10] Auffan M, Decome L, Rose J, Orsiere T, De Meo M, Briois V, et al. In vitro interactions between DMSA-coated maghemite nanoparticles and human fibroblasts: a physicochemical and cyto-genotoxical study. Environ Sci Technol 2006;40(14):4367–73.
[11] Berry CC, Charles S, Wells S, Dalby MJ, Curtis AS. The influence of transferrin stabilised magnetic nanoparticles on human dermal fibroblasts in culture. Int J Pharm 2004;269(1):211–25.
[12] Pisanic 2nd TR, Blackwell JD, Shubayev VI, Finones RR, Jin S. Nanotoxicity of iron oxide nanoparticle internalization in growing neurons. Biomaterials 2007;28(16):2572–81.
[13] Hamm B, Staks T, Taupitz M, Maibauer R, Speidel A, Huppertz A, et al. Contrast-enhanced MR imaging of liver and spleen: first experience in humans with a new superparamagnetic iron oxide. J Magn Reson Imaging 1994;4(5):659–68.
[14] Dias AM, Hussain A, Marcos AS, Roque AC. A biotechnological perspective on the application of iron oxide magnetic colloids modified with polysaccharides. Biotechnol Adv 2011;29(1):142–55.
[15] Laurent S, Forge D, Port M, Roch A, Robic C, Vander Elst L, et al. Magnetic iron oxide nanoparticles: synthesis, stabilization, vectorization, physicochemical characterizations, and biological applications. Chem Rev 2008;108(6):2064–110.
[16] Karlsson HL, Cronholm P, Gustafsson J, Moller L. Copper oxide nanoparticles are highly toxic: a comparison between metal oxide nanoparticles and carbon nanotubes. Chem Res Toxicol 2008;21(9):1726–32.
[17] Karlsson HL, Gustafsson J, Cronholm P, Moller L. Size-dependent toxicity of metal oxide particles–a comparison between nano- and micrometer size. Toxicol Lett 2009;188(2):112–8.
[18] Hanini A, Schmitt A, Kacem K, Chau F, Ammar S, Gavard J. Evaluation of iron oxide nanoparticle biocompatibility. Int J Nanomedicine 2011;6:787–94.
[19] Liu Y, Chen Z, Wang J. Systematic evaluation of biocompatibility of magnetic Fe_3O_4 nanoparticles with six different mammalian cell lines. J Nanoparticle Res 2010;13(1):199–212.
[20] Muller K, Skepper JN, Posfai M, Trivedi R, Howarth S, Corot C, et al. Effect of ultrasmall superparamagnetic iron oxide nanoparticles (Ferumoxtran-10) on human monocyte-macrophages in vitro. Biomaterials 2007;28(9):1629–42.
[21] Dizdaroglu M, Laval J, Boiteux S. Substrate specificity of the Escherichia coli endonuclease III: excision of thymine- and cytosine-derived lesions in DNA produced by radiation-generated free radicals. Biochemistry 1993;32(45):12105–11.

[22] Reddy P, Jaruga P, O'Connor T, Rodriguez H, Dizdaroglu M. Overexpression and rapid purification of Escherichia coli formamidopyrimidine-DNA glycosylase. Protein Expr Purif 2004;34(1):126–33.
[23] Griffiths SM, Singh N, Jenkins GJ, Williams PM, Orbaek AW, Barron AR, et al. Dextran coated ultrafine superparamagnetic iron oxide nanoparticles: compatibility with common fluorometric and colorimetric dyes. Anal Chem 2011;83(10):3778–85.
[24] Hondow N, Harrington J, Brydson R, Doak SH, Singh N, Manshian B, et al. STEM mode in the SEM: a practical tool for nanotoxicology. Nanotoxicology 2011; 5(2):215–27.
[25] Doak SH, Griffiths SM, Manshian B, Singh N, Williams PM, Brown AP, et al. Confounding experimental considerations in nanogenotoxicology. Mutagenesis 2009;24(4):285–93.
[26] Lunov O, Syrovets T, Buchele B, Jiang X, Rocker C, Tron K, et al. The effect of carboxydextran-coated superparamagnetic iron oxide nanoparticles on c-Jun N-terminal kinase-mediated apoptosis in human macrophages. Biomaterials 2010;31(19):5063–71.
[27] Fellows MD, O'Donovan MR, Lorge E, Kirkland D. Comparison of different methods for an accurate assessment of cytotoxicity in the in vitro micronucleus test. II: practical aspects with toxic agents. Mutat Res 2008;655(1–2): 4–21.
[28] Ellard S, Mohammed Y, Dogra S, Wolfel C, Doehmer J, Parry JM. The use of genetically engineered V79 Chinese hamster cultures expressing rat liver CYP1A1, 1A2 and 2B1 cDNAs in micronucleus assays. Mutagenesis 1991;6(6): 461–70.
[29] Jaruga P, Kirkali G, Dizdaroglu M. Measurement of formamidopyrimidines in DNA. Free Radic Biol Med 2008;45(12):1601–9.
[30] Riemer J, Hoepken HH, Czerwinska H, Robinson SR, Dringen R. Colorimetric ferrozine-based assay for the quantitation of iron in cultured cells. Anal Biochem 2004;331(2):370–5.
[31] Arbab AS, Wilson LB, Ashari P, Jordan EK, Lewis BK, Frank JA. A model of lysosomal metabolism of dextran coated superparamagnetic iron oxide (SPIO) nanoparticles: implications for cellular magnetic resonance imaging. NMR Biomed 2005;18(6):383–9.
[32] Soenen SJ, Himmelreich U, Nuytten N, Pisanic 2nd TR, Ferrari A, De Cuyper M. Intracellular nanoparticle coating stability determines nanoparticle diagnostics efficacy and cell functionality. Small 2010;6(19):2136–45.
[33] Clogston JD, Patri AK. Zeta potential measurement. Methods Mol Biol 2011; 697:63–70.
[34] Boyer C, Whittaker MR, Bulmus V, Liu J, Davis TP. The design and utility of polymer-stabilized iron oxide nanoparticles for nanomedicine applications. NPG Asia Mater 2010;2:23–30.
[35] Corchero JL, Villaverde A. Biomedical applications of distally controlled magnetic nanoparticles. Trends Biotechnol 2009;27(8):468–76.
[36] Lynch I, Cedervall T, Lundqvist M, Cabaleiro-Lago C, Linse S, Dawson KA. The nanoparticle-protein complex as a biological entity; a complex fluids and surface science challenge for the 21st century. Adv Colloid Interface Sci 2007; 134-135:167–74.
[37] Singh N, Jenkins GJ, Asadi R, Doak SH. Potential toxicity of superparamagnetic iron oxide nanoparticles (SPION). Nano Rev; 2010. doi:10.3402/nano.v1i0.5358.
[38] Wilhelm C, Billotey C, Roger J, Pons JN, Bacri JC, Gazeau F. Intracellular uptake of anionic superparamagnetic nanoparticles as a function of their surface coating. Biomaterials 2003;24(6):1001–11.
[39] Xing X, He X, Peng J, Wang K, Tan W. Uptake of silica-coated nanoparticles by HeLa cells. J Nanosci Nanotechnol 2005;5(10):1688–93.
[40] Mahmoudi M, Simchi A, Imani M, Shokrgozar MA, Milani AS, Hafeli UO, et al. A new approach for the in vitro identification of the cytotoxicity of superparamagnetic iron oxide nanoparticles. Colloids Surf B Biointerfaces 2010; 75(1):300–9.
[41] Petersen E, Nelson B. Mechanisms and measurements of nanomaterial-induced oxidative damage to DNA. Anal Bioanal Chem 2010;398(2):613–50.
[42] Wang L, Zhang J, Zheng Y, Yang J, Zhang Q, Zhu X. Bioeffects of CdTe quantum dots on human umbilical vein endothelial cells. J Nanosci Nanotechnol 2010; 10(12):8591–6.
[43] Shukla RK, Sharma V, Pandey AK, Singh S, Sultana S, Dhawan A. ROS-mediated genotoxicity induced by titanium dioxide nanoparticles in human epidermal cells. Toxicol in Vitro 2011;25(1):231–41.
[44] Karlsson HL, Holgersson A, Moller L. Mechanisms related to the genotoxicity of particles in the subway and from other sources. Chem Res Toxicol 2008; 21(3):726–31.
[45] Kruszewski M, Iwanenko T. Labile iron pool correlates with iron content in the nucleus and the formation of oxidative DNA damage in mouse lymphoma L5178Y cell lines. Acta Biochim Pol 2003;50(1):211–5.
[46] Petrat F, de Groot H, Rauen U. Subcellular distribution of chelatable iron: a laser scanning microscopic study in isolated hepatocytes and liver endothelial cells. Biochem J 2001;356(Pt 1):61–9.
[47] Gackowski D, Kruszewski M, Bartlomiejczyk T, Jawien A, Ciecierski M, Olinski R. The level of 8-oxo-7,8-dihydro-2'-deoxyguanosine is positively correlated with the size of the labile iron pool in human lymphocytes. J Biol Inorg Chem 2002;7(4–5):548–50.
[48] Chourpa I, Douziech-Eyrolles L, Ngaboni-Okassa L, Fouquenet JF, Cohen-Jonathan S, Souce M, et al. Molecular composition of iron oxide nanoparticles, precursors for magnetic drug targeting, as characterized by confocal Raman microspectroscopy. Analyst 2005;130(10):1395–403.